Nanoscale

RSC Publishing

COMMUNICATION

View Article Online
View Journal | View Issue

Cite this: *Nanoscale*, 2013, **5**, 8915

Received 13th April 2013
Accepted 15th July 2013

DOI: 10.1039/c3nr01847d

www.rsc.org/nanoscale

Sensing extremely limited H_2 contents by Pd nanogap connected to an amorphous InGaZnO thin-film transistor†

Young Tack Lee,‡[a] Hwaebong Jung,‡[b] Seung Hee Nam,[ac] Pyo Jin Jeon,[a] Jin Sung Kim,[a] Byungjin Jang,[b] Wooyoung Lee*[b] and Seongil Im*[a]

A palladium (Pd) nanogap-based thin-film has been connected to an electrically stable amorphous InGaZnO thin-film transistor, to form a hydrogen sensor demonstrating a dramatic sensing capability. As a result of the Pd connection to the transistor source, our sensor circuit greatly enhances the hydrogen-induced signal and sensing speed in the sense of output voltage, clearly resolving a minimum hydrogen content of 0.05%. When the nanogap-based Pd thin-film was connected to the transistor gate, an extremely limited hydrogen content of even less than 0.05% was visibly detected through gate voltage shifts. Our results exhibit the most promising and practical ways to sense extremely limited hydrogen contents, originating from two methods: transistor-to-Pd nanogap resistor and transistor-to-Pd nanogap capacitor coupling.

Hydrogen sensing has continually drawn great attention since it was regarded important in industrial safety, which claims that 3–4% of ambient H_2 is the margin to avoid explosion danger.[1–9] So, monitoring the ambient H_2 and detecting an even extremely small content of H_2 gas is not only important but also always requested, particularly with practical and simple sensing tools.[6,10–23] Very recently, we reported one of the most innovative H_2 sensors, using typical Pd thin-films but containing nanogaps which were created by mechanically stretching an elastomeric substrate.[20–23] The sensitivity of our nanogap-based sensor appeared very good, so that less than ~0.1% of H_2 gas molecules in a N_2 atmosphere might be detected by reading signal current. However, reading the detection current at such low H_2 content was not easy at all; in fact even 0.2% hydrogen gas was barely noted by current sensors. More scientific techniques to improve the detection capability is thus necessary. In the present work, we dramatically improved the H_2 sensing capability of the nanogap-based Pd sensor by connecting it to an electrically stable amorphous InGaZnO thin-film transistor (a-IGZO TFT) in two different ways: Pd connection to the TFT source and to the gate. The IGZO TFT was chosen, since it was stable enough to bear the gate bias stress during H_2 detection; it would eventually be integrated with our Pd sensor. As a result of the Pd connection to the TFT source, our sensor circuit greatly enhances the H_2-induced signal by three orders of magnitude in the sense of output voltage, clearly resolving a minimum hydrogen content of 0.05%. When the nanogap-based Pd sensor was connected to the TFT gate, an even lower H_2 content of less than 0.05% was visibly detected, but more interestingly through this study of TFT gate oxide capacitor-to-Pd nanogap capacitor coupling, the size of the nanogap distance was approximately estimated as an important result.

Polydimethylsiloxane (PDMS) elastomer was used as the substrate of the hydrogen gas sensor, to create nanocracks (or nanogap stripes) in the Pd thin-film (TF). The base resin (Sylgard 184, Dow Corning) was mixed with a curing agent at a volume ratio of 10 : 1 and was kept in the vacuum chamber for 10 min to evacuate any air bubbles. After then, the PDMS mixture was cured for 30 min on a hotplate at 423 K. In order to fabricate the hydrogen gas sensor, a 10 nm-thin Pd film was deposited on the PDMS substrate by using a DC magnetron sputtering system. After Pd deposition, the Pd–PDMS substrate was mounted onto a stretching machine and nanocracks were created under a tensile stress.[20–23] (ESI, Fig. S1†) Fig. 1a shows a schematic of the as-cracked Pd TF device (area dimension: 10 mm [L] × 20 mm [W]), where many nanogap stripes are shown and one of them is illustrated in Fig. 1b with its schematic cross section. The single nanocrack appears deformed but yet maintains an internal connection (the connection was confirmed by an electric conduction measurement). However, if the initially cracked region comes into contact with H_2 gas molecules (*i.e.* is exposed to H_2 to form a PdH_x compound; Fig. 1c) and the molecules are evacuated, the crack is left

[a]*Institute of Physics and Applied Physics, Yonsei University, Seoul 120-749, Korea. E-mail: semicon@yonsei.ac.kr; Fax: +82-2-392-1592; Tel: +82-2-2123-2842*

[b]*Department of Materials Science and Engineering, Yonsei University, Seoul 120-749, Korea. E-mail: Wooyoung@yonsei.ac.kr; Fax: +82-2-312-5275; Tel: +82-2123-2834*

[c]*R&D Center, LG Display, Paju 413-811, Korea*

† Electronic supplementary information (ESI) available. See DOI: 10.1039/c3nr01847d

‡ These authors contributed equally to this work.

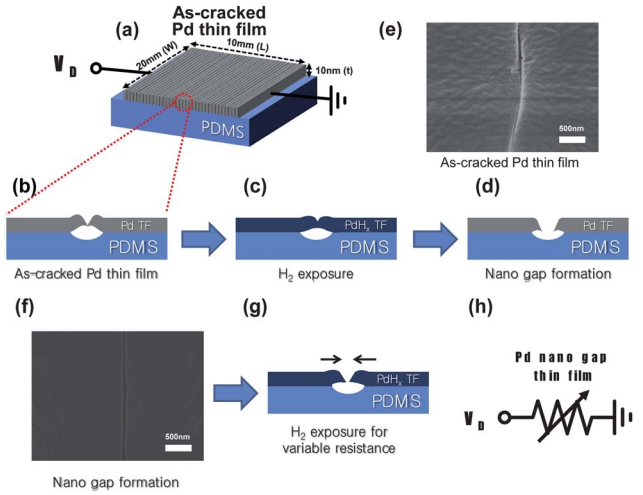

Fig. 1 Schematics of (a) an as-cracked Pd TF device, (b) an as-cracked nanogap stripe in cross sectional view, (c) a PdH_x compound-containing stripe as exposed to H_2, and (d) the stripe with an eternally open nanogap. SEM images of (e) and (f) show a stripe from the as-cracked and eternal nanogap-containing Pd TF, respectively. (g) A schematic cross section of a nanogap stripe in Pd TF with variable electrical resistances which depend on H_2 exposure, and (h) its equivalent circuit.

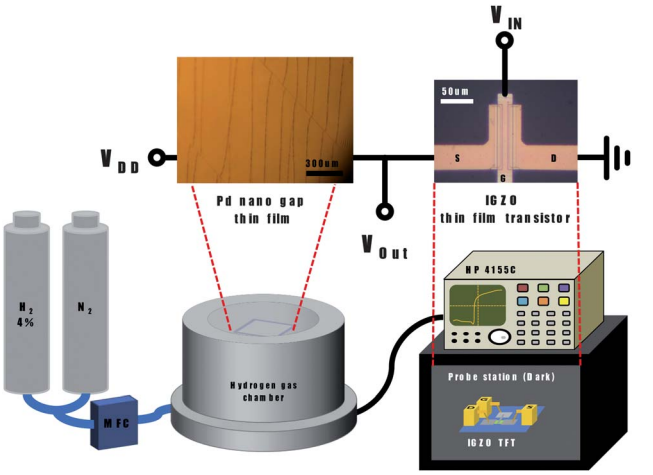

Fig. 2 Schematic illustration of our H_2 sensor system. The nanogap Pd TF device was mounted in the gas chamber and connected to an electrically stable a-IGZO TFT device of a probe station in the dark. Optical microscope images for a nanogap-stripe Pd TF resistor and TFT are presented in the inverter type circuit.

eternally open with a nanogap as shown in Fig. 1d. Fig. 1e and f are the respective scanning electron microscopy (SEM) images of as-cracked and eternal nanogap-containing Pd TF. According to the SEM images, the as-cracked Pd still shows a physical contact between the two Pd regions around the crack stripe while the other stripe from nanogap-containing Pd shows ~50 nm separation (gap distance), although the distance is not uniform. Based on the structure of Fig. 1d and f, the nanogap Pd TF now operates as a H_2 sensor, since ON/OFF (contact/no contact) switching takes place in the Pd TF with variable resistances according to the degree of H_2 molecule adsorption on the Pd surface or H_2 reaction with Pd. The H_2-adsorbed Pd TF changes its phase to PdH_x with an expanded volume which leads to a physical contact in the nanogap (see the illustration in ESI, Fig. S2†).[24–27] As a result, the variable electrical conductance of nanogap Pd TF may indicate H_2 content (see Fig. 1g and h for the illustration and circuit of the variable resistance).

The structure of a-IGZO TFTs is an inverted-stagger type with a width-to-length (W/L) ratio of 100 : 10 μm using a bottom gate (ESI, Fig. S3†). A 300 nm-thick SiO_2 gate insulator layer was deposited on the patterned Cu–MoTi gate electrode by a plasma-enhanced chemical vapor deposition (PECVD) system. Then, a 60 nm-thick active channel layer (a-IGZO) was deposited by a DC magnetron sputtering system. The formation of the SiO_2 etch stopper (75 nm) and Mo source/drain electrodes were sequentially performed, followed by the formation of a 300 nm-thick PECVD SiO_2 passivation layer. All the patterning processes were carried out by photolithography that involved wet chemical etching and PECVD processes. The device annealing at 300 °C in ambient air was performed as a final process.

Fig. 2 shows a schematic diagram of our H_2 sensor system, which consists of a small gas chamber with a volume of ~250 ml and a mass flow controller (MFC) for pure 100% N_2 (for purging) and 96% N_2 + 4% H_2 mixture gas (for sensing). The pressure in the chamber was maintained at 1 atm at room temperature. The nanogap Pd TF device was mounted in the gas chamber and connected to an electrically stable a-IGZO TFT device (to the source electrode) of a probe station in the dark. Supply and input voltages (V_{DD} and V_{IN}) were applied by a semiconductor parameter analyzer (Model HP 4155C, Agilent Technologies). Output voltage (V_{OUT}) according to H_2 sensing was also measured by the semiconductor analyzer. The circuit illustration in Fig. 2 contains the top view images of our nanogap Pd TF device and a-IGZO TFT, which were obtained from an optical microscope. As shown, our Pd TF contains many nanogap stripes, of which the number was approximated to be 60–70. Our measurement setup is analogous to a logic inverter circuit for digital output, except that ours has a variable resistor composed of a H_2-sensing nanogap Pd TF instead of a constant load resistor; we could thus expect that small H_2-induced analogue current would be properly amplified in voltage signals.

Fig. 3a is a detecting current *vs.* time plot which is obtained from our nanogap Pd TF (under 0.1 V) by H_2 gas-controlled ON/OFF switching. Various H_2 ambiences of 4%, 2%, 1%, 0.5%, 0.4%, 0.3%, and 0.2% (as mixed with pure N_2) were exposed to the Pd sensor. While H_2 concentrations higher than 0.3% were quite nicely detected at the current range from ~2 mA to few hundred μA, it was not easy to note a lower H_2 content from the current signal. In particular, 0.2% H_2 was barely sensed and noted only by magnifying the sensing signal (~200 nA) as shown in the inset of Fig. 3a. Worse than that, sensing (and recovery) time gets longer with smaller H_2 content, so that detecting 0.3% H_2 appeared to take more than 20 s. Hence, we employed an electrically stable a-IGZO TFT to amplify the sensing signal and simultaneously to shorten the sensing time, converting the output signal from current to voltage. Fig. 3b is the drain current–gate voltage (I_D–V_G) transfer characteristics of our oxide TFT along with gate leakage current (I_G) curves, as

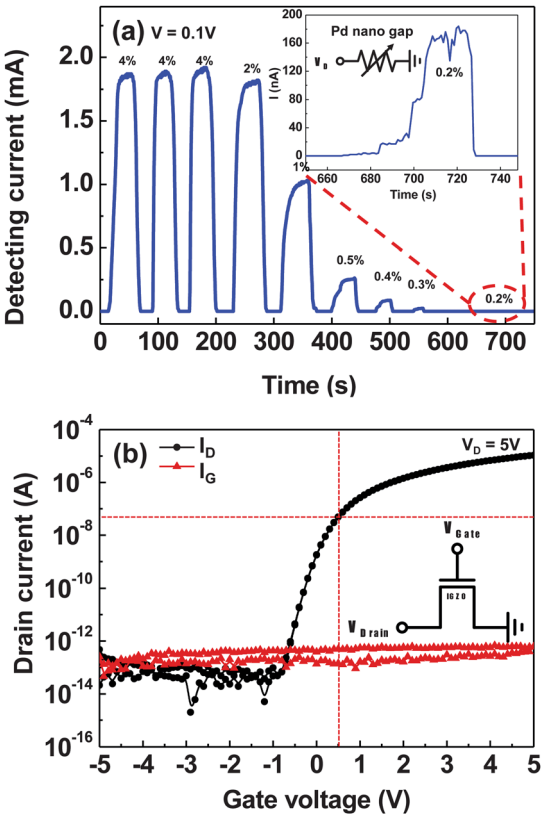

Fig. 3 (a) Detecting current *vs.* time plot achieved by H_2 gas-controlled ON/OFF switching in nanogap Pd TF. Various H_2 contents of 4%, 2%, 1%, 0.5%, 0.4%, 0.3%, and 0.2% were exposed to the Pd sensor and purged by pure N_2. Inset shows the current for 0.2% H_2 in zoomed scale. (b) Drain current–gate voltage (I_D–V_G) transfer characteristics of our a-IGZO TFT device.

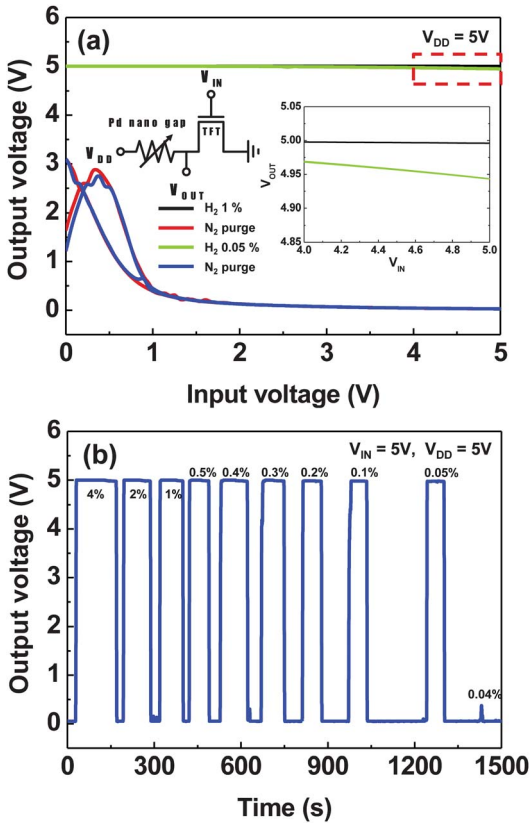

Fig. 4 (a) V_{OUT} *vs.* V_{IN} plots of our inverter type H_2 sensor tested with 1%, 0.05%, and 0% (pure N_2) of H_2 contents. The inset shows the V_{OUT} curves for 1 and 0.05% H_2 in zoomed scale. (b) Dynamic H_2 detection plot in time domain for various H_2 contents from 4% to 0.05%.

obtained under a drain bias of V_D = 5 V. As shown in the TFT transfer curves of Fig. 3b, our TFT was very stable with 0.1 pA I_G leakage and without any gate hysteresis, turning on above 0 V. (ON/OFF ratio was more than ~108 and the saturation field-effect mobility was ~10 $cm^2\ V^{-1}\ s^{-1}$). Since the transistor I_D current covers a broad range from 20 μA to 0.1 pA while our Pd sensor has another current range from 2 mA to a few hundred nA, some reasonable V_{OUT} signals are expected through an overlapped current region when these two devices are connected in series.

The series connection scheme has already been introduced in Fig. 2 and is now shown in the inset circuit diagram of Fig. 4a, where V_{OUT} *vs.* V_{IN} plots are displayed as the main measurement results. For H_2 detection experiments, H_2 gas of 1%, 0.05%, and 0% (purged with 100% N_2 gas) was infused into the hydrogen sense chamber of Fig. 2 in the following sequence: initial 1% H_2 infusion, N_2 purge, 0.05% H_2 infusion, and final N_2 purge, so that each V_{OUT} curve could be obtained under a V_{DD} of 5 V as shown in Fig. 4a. According to the plots, the V_{OUT} for 0.05% H_2 detection appears almost the same as that for 1% H_2 sensing, indicating almost 5 V; this result is confirmed by magnifying some part of the plot (see the inset plot for a range of V_{IN} = 4–5 V). Without H_2 (by N_2 purge), V_{OUT} drops to 0 V at a high V_{IN}, however the drop stops near ~2.5 V at a low V_{IN} of 0.5 V, which might be too low to open the transistor channel properly. Based on these V_{OUT}–V_{IN} plots, we implemented a time domain H_2 detection experiment (for V_{OUT} *vs.* time plot), dynamically varying the H_2 concentration from 4% to 0.04% under a fixed voltage condition of V_{DD} = V_{IN} = 5 V. Fig. 4b displays the dynamic H_2 detection plot in time domain, where the detection voltage V_{OUT} appears to be ~5 V for all the cases from 4% to 0.05% H_2, as predicted by the results from Fig. 4a. (The results in Fig. 4b were reproducible and a magnified time domain V_{OUT} plot is seen in the ESI, Fig. S4.†) The detection voltage abruptly decreases to 0.4 V from ~5 V when the H_2 content further decreases to 0.04%, although this specific result was actually irreproducible unlike the case of 0.05% and higher H_2 percentages. We thus recognize that the series connection setup for H_2 sensing still has its own detection limit at 0.05%. In spite of such a limitation, however, it is acknowledgeable that applying our logic inverter type circuit to the analogue nanogap Pd TF remarkably enhances the visibility of the low % H_2 signal by a few orders of magnitude and simultaneously shortens the sensing (and recovery) time to 1–2 s. In fact, the electrical conductance or conducting path in nanogap Pd film still exists even with the low 0.05% hydrogen molecules, but is too small to measure/or estimate and thus becomes visible only with the connection to a transistor. Apparent electrical disconnection in the nanogap Pd film is eventually observed with an extremely

low % of H_2 molecules (here 0.04% is the onset point of the open circuit).

Complete gap opening might take place in single or a few nanogap stripes at a certain point of dilute ambient H_2, leading to an abrupt disconnection. In this event, our nanogap-containing Pd TF has then a charge capacitance due to the gap distance. The gap distance would be so dependent on the H_2 content that we may estimate an extremely low % of H_2 by introducing the capacitance of the nanogap Pd TF to the gate of the same a-IGZO TFT with a dielectric oxide (300 nm thick SiO_2). Such a capacitor-induced circuit is shown in the inset of Fig. 5a and the transfer curves have been accordingly obtained from the circuit with the oxide TFT and Pd TF variable capacitor under two ambient conditions of 0.04% and 0% H_2 (by N_2 purge). The initial transfer curve was obtained as a reference from the TFT alone. Connected in series to the Pd TF, the total gate capacitance (C_{total}) of the inset circuit should become smaller than the dielectric oxide capacitance C_{ox} because a nanogap-induced capacitance (C_{gap}) should be also considered as shown below in eqn (1).

$$C_{total} = \frac{1}{\left(\frac{1}{C_{gap}} + \frac{1}{C_{ox}}\right)} \quad (1)$$

The smaller C_{total} leads to a slightly smaller I_D current than that by C_{ox} alone at an identical on-state V_G (*e.g.* 3 V), as shown in Fig. 5a. Simultaneously, at the same off-state I_D (*e.g.* ~0.3 pA) the smaller C_{total} leads to a more negative V_G, that is, the transfer curves of the TFT with the Pd TF capacitor shows more negatively shifted V_G with a lower H_2 content, since the C_{gap} makes an additional charging and voltage drop ($V_{gap} = V_G - V_{Gi}$) prior to C_{ox}-induced gate charging. The C_{gap} can be expressed as $A\varepsilon_0/d$, where A is the thickness of the wall area of a nanogap stripe (10 nm × 20 mm), d is the gap distance, and ε_0 is the dielectric constant in air (or N_2). The V_{gap} is measured from the transfer curves where an off-state voltage (V_{Gi}) of the initial TFT is indicated by a dashed line of Fig. 5a. These V_G shift results may provide a key solution for sensing even an extremely low H_2% and simultaneously for the estimation of the H_2%-dependent average gap distance as well. Using the V_{gap} and C_{gap} dependence on H_2%, we estimated the average gap distances in 0% and 0.04% H_2 ambiences to be ~30 nm and ~9 nm, respectively. Since the circuit is connected to the gate through the Pd TF resistor anyway if the H_2 content in the chamber atmosphere is over 0.05%, the transfer curves under such conditions become almost identical to the initial transfer curve obtained without the Pd TF connection; in fact Fig. 5b displays the two curves quite overlapped on the initial curve. An equivalent circuit is shown in the inset of Fig. 5b, where the nanogap Pd TF is expressed as a variable resistor. Fig. 5c and d are the respective illustrations of Pd TF capacitor and resistor models with diluted and concentrated H_2 molecules in a Pd lattice.

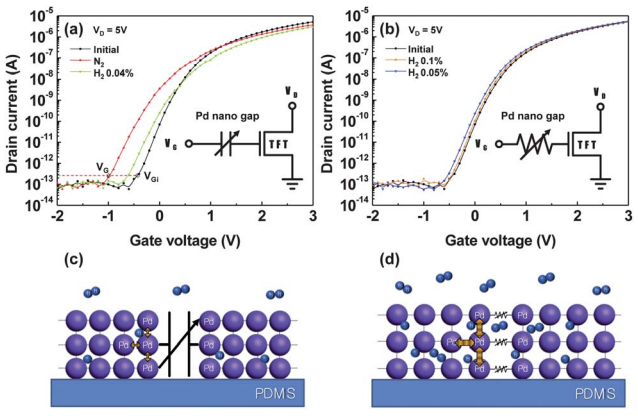

Fig. 5 (a) I_D–V_G Transfer curves obtained from the initial a-IGZO TFT (black line) and from the a-IGZO TFT linked to the Pd TF variable capacitor under two ambient conditions: 0% H_2 (pure N_2; red line) and 0.04% H_2 (green line). Inset is the corresponding equivalent circuit with the capacitor. (b) I_D–V_G transfer curves obtained from the a-IGZO TFT device (black line) and from the a-IGZO TFT linked to the Pd TF variable resistor in another two ambiences: 0.1% (orange line) and 0.05% H_2 (blue line). Inset is the corresponding circuit with the resistor. Illustrations (c) and (d) are the respective models of Pd TF capacitor and resistor with diluted and concentrated H_2 molecules in a Pd lattice.

Merging the TFT gate oxide and nanogap Pd TF capacitors, the total gate capacitance (C_{total}) becomes smaller than the dielectric oxide capacitance (here C_{ox} for 300 nm thick SiO_2). We already addressed this point in eqn (1), since a nanogap-induced capacitance (C_{gap}) should be considered in addition to C_{ox}. At the same off-state I_D (*e.g.* ~0.3 pA) an open circuit-based transfer curve shows more negatively shifted V_G, since the C_{gap} makes an additional charging and voltage drop ($V_{gap} = V_G - V_{Gi}$) prior to C_{ox}-induced gate charging. A schematic circuit of this situation is illustrated in Fig. 6. The following eqn (2)–(4) are now useful for the estimation of the nanogap distance. Due to a series capacitance theory in general physics,

$$Q_{gap} = Q_{ox} = Q_s, \quad (2)$$

and

$$C_{gap}V_{gap} = C_{ox}V_{ox} = 2C_s\Psi_s \quad (3)$$

then,

$$V_{Gi} - V_{FB} = V_{ox} + \Psi_s + V_c, \quad (4)$$

where Q_{gap} (= $C_{gap}V_{gap}$), Q_{ox} (= $C_{ox}V_{ox}$), and Q_s (= $2C_s\Psi_s$) are total charges in the nanogap, oxide–gate interface, and depleted a-IGZO film, respectively. Eqn (4) is from the TFT without the Pd TF capacitor. V_{Gi} is an initial off-state gate voltage of the TFT

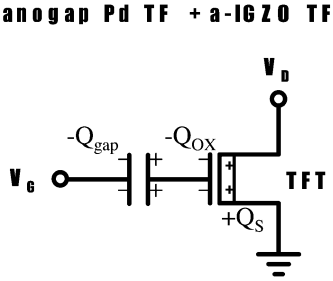

Fig. 6 A circuit to express the series capacitance theory, with eqn (2) and (3) in a merged system of the TFT gate oxide and nanogap Pd TF capacitor.

without the Pd TF capacitor, V_{FB} is the flat band voltage, Ψ_s is a voltage for semiconductor band bending for an off-state (semiconductor charge depletion), V_{ox} is the band bending of the dielectric SiO_2, V_c is an average channel voltage ($<V_D = 5$ V), and C_s is the capacitance of a charge-depleted 60 nm-thin a-IGZO semiconductor. (Note that Q_{gap} ($= C_{gap}V_{gap}$) and Q_{ox} ($= C_{ox}V_{ox}$) are sheet charges but Q_s ($= 2C_s\Psi_s$) is the charge in a thin film; that is why the factor of 2 is added.)[28] Whether the Pd TF capacitor is connected or not, the same band bending terms (V_{ox} and Ψ_s) should be maintained in both cases for a transistor (with and without the Pd TF capacitor) to keep an identical off-state current I_D (~3 pA). Now, from the capacitance–voltage (C–V) curve of Fig. 7, we may extract a part of eqn (4), $V_{ox} + \Psi_s$ since in C–V measurements V_{FB} is approximated by the cross point of two tangent lines while V_c is zero so that V_{Gi} becomes V_{Go}; $V_{ox} + \Psi_s$ is ~−1.0 V as estimated from $V_{Go} - V_{FB}$ in the C–V curve. The minimum C_{total} in the C–V curve is observed to be ~0.025 pF ($= 1/(1/C_s + 1/C_{ox})$, eqn (1)) in a depletion state and C_{ox} is measured to be ~0.131 pF in an accumulation state of V_G (the inset band diagrams respectively indicate the depletion and accumulation states). As a result from eqn (1), C_s is calculated to be ~0.031 pF, since we measure the C_{ox} from the C–V curve. Then we use the relation $C_{ox}V_{ox} = 2C_s\Psi_s$ along with another relation $V_{ox} + \Psi_s = \sim -1.0$ V, to work out V_{ox} and Ψ_s (−0.32 V and −0.68 V, respectively). Since our Pd TF stripe area (A) is 10 nm × 20 mm (for $t \times W$, see Fig. 1a) and it can be applied to eqn (3), we can finally estimate the gap distance using another equation below,

$$C_{gap} = \frac{\varepsilon_0 A}{Nd} = \frac{C_{ox}V_{ox}}{V_{gap}}. \quad (5)$$

Now,

$$Nd = \frac{\varepsilon_0 A V_{gap}}{C_{ox}V_{ox}}, \quad (6)$$

where N is the number of nanogap stripes playing as capacitors in Pd TF, d is the gap distance of a single capacitor, V_{gap} is 0.7 V for N_2 purge conditions and 0.22 V for 0.04% H_2 according to Fig. 5a. Average Nd values are calculated to be ~30 nm and ~9 nm for the above two respective cases (0% and 0.04% H_2). N might be 1 or more, but here it is very likely that N is 1 for the 0.04% case, since we have observed an abrupt electrical disconnection at 0.04% H_2 with only a little dilution of H_2 from 0.05 to 0.04%. The maximum gap distance would be ~30 nm as in the case of 0% H_2. Our calculation of the gap distances may not provide an exact number value, however, the calculated value is at least comparable to the scale observed in the SEM results of Fig. 1f.

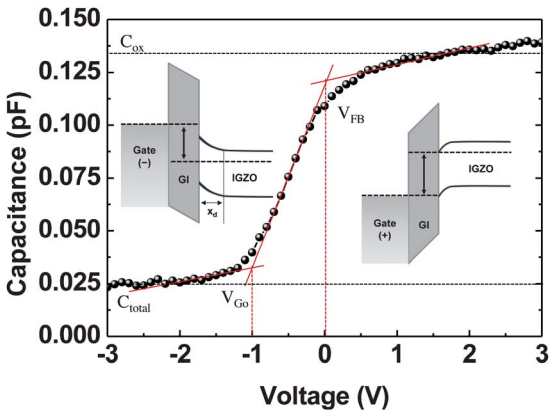

Fig. 7 Capacitance–voltage (C–V) curve obtained from our a-IGZO TFT device. For this C–V measurement, S/D electrodes were used as the ground. Inset band diagrams respectively indicate the depletion and accumulation states of the device. V_{FB} and V_{Go} were estimated by finding the cross point between two tangent lines, as shown above.

Conclusions

In summary, we have fabricated an ultrasensitive H_2 sensor system composed of an electrically stable a-IGZO TFT and a nanogap-containing Pd TF, which acts as an analogue variable resistor depending on the H_2 content. By connecting the nanogap Pd TF to the TFT source, our inverter type sensor circuit greatly enhances the H_2-induced signal visibility and sensing speed in a sense of output voltage, clearly resolving a minimum hydrogen content of 0.05%. When the nanogap-based Pd TF was connected to the TFT gate, an even lower H_2 content of less than 0.05% was visibly detected, since the Pd TF acts as a capacitor with H_2-dependent variable capacitance. We thus conclude that our system of oxide TFT-coupled Pd TF with nanogaps is very promising for sensing an extremely low H_2 content in the ambient atmosphere.

Acknowledgements

Authors acknowledge the financial support from NRF grant (NRL program: Grant no. 2009-0079462) and Priority Research Centers Program (2009-0093823) through the National Research Foundation of Korea(NRF). Young Tack Lee would like to thank for the LGenius Members Fellowship from LGD company.

Notes and references

1 A. Katsuki and K. Fukui, *Sens. Actuators, B*, 1998, **52**, 30.
2 K. I. Lundström, M. S. Shivaraman and C. M. Svensson, *J. Appl. Phys.*, 1975, **46**, 3876.
3 B. S. Kang, R. Mehandru, S. Kim, F. Ren, R. C. Fitch, J. K. Gillespie, N. Moser, G. Jessen, T. Jenkins, R. Dettmer, D. Via, A. Crespo, B. P. Gila, C. R. Abernathy and S. J. Pearton, *Appl. Phys. Lett.*, 2004, **84**, 4635.
4 M. Yun, N. V. Myung, R. P. Vasquez, C. Lee, E. J. Menke and R. M. Penner, *Nano Lett.*, 2004, **4**, 419.
5 Y. Im, C. Lee, R. P. Vasquez, M. A. Bangar, N. V. Myung, E. J. Menke, R. M. Penner and M. Yun, *Small*, 2006, **2**, 356.
6 F. Favier, E. C. Walter, M. P. Zach, T. Benter and R. M. Penner, *Science*, 2001, **293**, 2227.
7 M. Z. Atashbar and S. Singamaneni, *Sens. Actuators, B*, 2005, **111–112**, 13.
8 J. Kong, M. G. Chapline and H. Dai, *Adv. Mater.*, 2001, **13**, 1384.
9 Y. Sun and H. H. Wang, *Appl. Phys. Lett.*, 2007, **90**, 213107.
10 R. Dasari and F. P. Zamborini, *J. Am. Chem. Soc.*, 2008, **130**, 16138.

11 T. Kiefer, F. Favier, O. Vazquez-Mena, G. Villanueva and J. Brugger, *Nanotechnology*, 2008, **19**, 125502.
12 S. Mubeen, B. Yoo and N. V. Myung, *Appl. Phys. Lett.*, 2008, **93**, 133111.
13 F. J. Ibanez and F. P. Zamborini, *J. Am. Chem. Soc.*, 2008, **130**, 622.
14 E. C. Walter, F. Favier and R. M. Penner, *Anal. Chem.*, 2002, **74**, 1546.
15 F. Yang, D. K. Taggart and R. M. Penner, *Nano Lett.*, 2009, **5**, 2177.
16 S. Cherevko, N. Kulyk, J. Fu and C. Chung, *Sens. Actuators, B*, 2009, **136**, 338.
17 M. Khanuja, S. Kala, B. R. Mehta and F. E. Kruis, *Nanotechnology*, 2009, **20**, 015502.
18 T. Kiefer, L. G. Villanueva, F. Fargier, F. Favier and J. Brugger, *Nanotechnology*, 2010, **21**, 505501.
19 M. Z. Atashbar, D. Banerji and S. Singamaneni, *IEEE Sens. J.*, 2005, **5**, 792.
20 J. Lee, W. Shim, E. Lee, J. Noh and W. Lee, *Angew. Chem., Int. Ed.*, 2011, **50**, 5301.
21 J. Lee, J. Noh, S. H. Lee, B. Song, H. Jung, W. Kim and W. Lee, *Int. J. Hydrogen Energy*, 2012, **37**, 7934.
22 T. Chang, H. Jung, B. Jang, J. Lee, J. Noh and W. Lee, *Sens. Actuators, A*, 2013, **192**, 140.
23 H. Jung, B. Jang, W. Kim, J. Noh and W. Lee, *Sens. Actuators,B*, 2013, **178**, 689.
24 R. Feenstra, G. J. Bruin-Hordijk, H. L. M. Bakker, R. Griessen and D. G. Groot, *J. Phys. F: Met. Phys.*, 1983, **13**, L13.
25 Y. Sakamoto, K. Takai, I. Takashima and M. Imada, *J. Phys.: Condens. Matter*, 1996, **8**, 3399.
26 A. L. Cabrera and R. Aguayo-Soto, *Catal. Lett.*, 1997, **45**, 79.
27 Y. Okuhara, Y. Imai, Y. Noguchi and M. Takata, *Bull. Mater. Sci.*, 1999, **22**, 999.
28 R. S. Muller, T. I. Kamins and M. Chan, *Device Electronics for Integrated Circuits*, John Wiley & Sons, New York, 3rd edn, 2002, pp. 390–396.